# Effect of the Variation in the Weight Percentage of the Loading and the Reduction in the Nanosizes of $CaSO_4$ on the Mechanical and Thermal Properties of Styrene–Butadiene Rubber

**S. Mishra, N. G. Shimpi**

*University Department of Chemical Technology, North Maharashtra University, P.O. Box 80, Jalgaon 425 001 MS India*

Received 18 February 2006; accepted 17 May 2006
DOI 10.1002/app.25910
Published online in Wiley InterScience (www.interscience.wiley.com).

**ABSTRACT:** The incorporation of fillers into elastomers has profound effects on the mechanical, physical, and thermal properties of the nanocomposites that form. In this study, styrene–butadiene rubber as a matrix was reinforced separately with 10-, 15-, or 23-nm $CaSO_4$, which was synthesized by an *in situ* deposition technique. The mixing and compounding were performed on a two-roll mill, and sheets were prepared in a compression-molding machine. Properties such as the swelling index, specific gravity, tensile strength, elongation at break, modulus at 300% elongation, Young's modulus, hardness, and abrasion resistance were measured. The morphology of the rubber nanocomposites was also performed with scanning electron microscopy to study the dispersion of the nanofiller in the rubber matrix. The thermal decomposition of the rubber nanocomposites was studied with thermogravimetric analysis, and the results were compared with those of commercial $CaSO_4$-filled styrene–butadiene rubber. A reduction in the nanosizes of $CaSO_4$ led to an enhancement of the mechanical, physical, and thermal properties of the rubber nanocomposites. Above a 10 wt % filler loading, the styrene–butadiene rubber showed a reduction in all properties. This effect was observed because of the agglomeration of the nanoparticles in the rubber matrix. The thermodynamic parameters were also studied.  J Appl Polym Sci 104: 2018–2026, 2007

**Key words:** elastomers; flame retardance; mechanical properties; nanoparticles; TEM; thermal properties; thermodynamics

## INTRODUCTION

Nanosize particles, which have attracted great attention for the past few decades, have attractive characteristics in comparison with microsize particles. The surface area is very large, and the percentage of molecules or atoms on the surface is greatly increased because of the very small size. This is expected to have wide applications in various fields. Nanotechnology is recognized as a technology development for the 21st century. In the industry of materials, the development of ceramic and polymer nanocomposites is a rapidly expanding, multidisciplinary research activity.

Composite materials are made of two or more components consisting of two or more phases. They are divided into three categories: (1) particulate-filled composites, (2) fiber-filled composites, and (3) interpenetrating network composites. Polymer nanocomposites represent a new alternative to conventionally filled polymers with less than 5% of their addition in the matrix. Because of their nanometer sizes, filler dispersions in nanocomposites exhibit markedly improved properties in comparison with pure polymers or their traditional composites. Polymer–clay nanocomposites are a rapidly developing class of materials. These nanocomposites have attracted great attention since the Toyota group[1] incorporated layered silicates into nylon, which showed an enhancement in its properties. Even the amount of clay is much less in the polymer; however, the matrix shows improvements in the mechanical properties,[2] solvent resistance,[3] ionic conductivity,[4] flammability resistance,[5] gas-barrier properties,[6] and biodegradability of biodegradable polymers.[7] Numerous researchers have already worked on clay nanocomposites based on a variety of polymers.[8–18] In our earlier studies, we used inorganic nanofillers in various matrices, which showed considerable enhancements in the mechanical, thermal, and physical properties.[19–23] The purpose of this study was to investigate

Part of this article was presented at the National Conference on Recent Trends in Chemical Technology, January 6–7, 2006, at North Maharashtra University (Jalgaon, India).

*Correspondence to:* S. Mishra (profsm@rediffmail.com).

Contract grant sponsor: Council of Scientific and Industrial Research (New Delhi, India); contract grant number: 01(2018)/05/EMR-II.

the effects of nanoparticles of $CaSO_4$ on the mechanical, thermal, and physical properties of styrene–butadiene rubber (SBR).

## EXPERIMENTAL

### Materials

SBR (Hyundai Techlen 1502, Goodyear Tyre & Rubber Co., Oxford, US) was used. The physical properties of SBR are listed in Table I. The rubber additives—stearic acid, zinc oxide (ZnO), zinc diethyl dithiocarbamets (ZDC), 2,2′-dibenzothiazyl disulfide (MBTS), phenyl-β-naphthyl amine (Vulconex), and sulfur—all commercial-grade, were procured from Bayer India Ltd. (Mumbai, India). An analytical grade of calcium chloride, ammonium sulfate, and poly(ethylene glycol) (PEG; molecular weight = 6000) were procured from Qualigens India, Ltd. (Mumbai, India) and were used for the synthesis of nanoparticles of calcium sulfate. The particle size of commercial $CaSO_4$ was 40 μm.

### Synthesis and characterization of the nanoparticles

Nano-$CaSO_4$ was synthesized by a matrix-mediated process. The details of the synthesis are given elsewhere;[19–23] here ammonium carbonate was s replaced by ammonium sulfate to obtain nano-$CaSO_4$. The nanosizes were confirmed with an X-ray diffractometer (Rigaku, Tokyo, Japan) with an intensity in the range of 0–6000 cps and a diffraction angle of 0–35°. The particle sizes were determined with Scherrer's formula: particle size (Å) = $k\lambda/\Delta 2\theta \cos\theta$, where $k$ is the order of reflection, $\lambda$ is 1.542, $\theta$ is the diffraction angle, and $\Delta 2\theta$ is the full width at half-maximum. The particle sizes of $CaSO_4$ obtained from 4 : 1, 20 : 1, and 32 : 1 ratios of PEG to calcium chloride were recorded as 23, 15, and 10 nm, respectively.

The formulation for the rubber compounds was as follows: 100 g of SBR, 3 g of stearic acid, 3 g of ZnO, 1 g of Vulconex, 0.5 g of ZDC, 0.5 g of MBTS, 1.8 g of sulfur, and various amounts of nano-$CaSO_4$. Rubber was masticated on a two-roll mill for 2–3 min, and then stearic acid was added to give flexibility to the raw rubber. After the complete addition of stearic acid, ZnO was added, following MBTS and ZDC, which acted as the activator and accelerator; further mixing was performed for 1–2 min. Later, Vulconex was added as an antioxidant. After sufficient mastication, sulfur was added. At last, nano-$CaSO_4$ was added very carefully because of its very fine size. The same procedure was followed for commercial $CaSO_4$ as a filler. The compounded rubber was subjected to compression molding for 40 min at 140°C under 100 kg/cm$^2$ of pressure to get a square sheet of $15 \times 15 \times 0.3$ cm$^3$.

**TABLE I**
**Physical Properties of SBR**

| No. | Property | Value |
|---|---|---|
| 1 | Appearance | Light tan/black |
| 2 | Bound styrene | 23.5% |
| 3 | Organic acid | 6.5% |
| 4 | Mooney viscosity | 50 mL (100°C) |
| 5 | Specific gravity | 0.94 g/cc |

### Thermal degradation

Thermal degradation measurements were carried out on a Shimadzu (Tokyo, Japan) TGA 50 thermogravimetric analyzer. Temperature programming was performed from 0 to 600°C at a heating rate of 10°C/min under a nitrogen atmosphere to remove all corrosive gases and to avoid thermooxidative degradation.

### Swelling index

The swelling index, an indirect way of measuring the total crosslink density, which in turn is correlated to the physical properties of the various vulcanizates, was determined through the swelling of a sample in toluene for 24 h at room temperature. It was calculated with the following equation:[22–24]

$$\text{Swelling index} = (X - Y)/Y$$

where $X$ is the weight of the sample after swelling and $Y$ is the weight of the sample before swelling.

### Specific gravity

An analytical balance equipped with a stationary support for an immersion vessel above or below the balance pan was used for specific gravity measurements per ASTM D 792. Corrosion-resistant wire for suspending a specimen and a sinker for a lighter specimen with a specific gravity of less than 1 was employed. A beaker was used as an immersion vessel, a test specimen of convenient size was weighed in air, and then the specimen was suspended from a fine wire attached to the balance. The sample was completely immersed in distilled water. The weight of the specimen in water was determined (with the sinker). The specific gravity of the specimen was calculated as follows:

$$\text{Specific gravity of specimen} = a/[(a + w) - b]$$

where $a$ is the weight of the specimen in air, $b$ is the weight of the specimen (with the sinker) and wire in water, and $w$ is the weight of the totally immersed sinker and partially immersed wire.

### Mechanical testing

The cured sheets were subjected to conditioning for 24 h at a relative humidity of 50%. The mechanical

properties, such as the tensile strength, elongation at break, and modulus at 300%, were measured per ASTM D 412 with a universal testing machine (UTM 2302) supplied by R&D Equipment (Mumbai, India). The crosshead speed was 50 mm/min. The samples were of standard dumbbell shape. All measurements were performed eight times to obtain the average value.

### Flame retardancy

The flame-retardancy test was carried out with a Prolific flame tester (Noida, Uttar Pradesh, India) per ASTM D 4804. The sample was clamped 85 mm above the horizontal screen so that it would not sag and touch the screen. A free end was exposed to a specified gas flame for 30 s. The sample was clamped at a 45° angle with a flame tip. The time required for the burning and the relative rate of burning were measured.

### Hardness testing

The compression-molded specimens were tested to report the hardness data with a Shore A hardness tester per ASTM D 2240.

### Abrasion resistance

The abrasion resistance index test was carried out on a Prolific rotating-drum abrasion tester per the IS 3400 standard. A test specimen of 16 ± 0.2 $mm^2$ was gripped in the specimen holder in such a manner that it projected 2 ± 0.2 mm beyond the face on the grip. The cylinder was rotated at 40 rpm.

### Scanning electron microscopy (SEM)

To study the extent of the dispersion and agglomeration of the nanofiller into the rubber matrix, SEM studies were carried out on a Cemeca (Paris, France) model SU-30 instrument.

### Transmission electron microscopy (TEM)

TEM (Tokyo, Japan) of $CaSO_4$ was recorded on a Hitachi H-800 transmission electron microscope for the confirmation of the dimensions and shapes of the nanoparticles. The nanoparticles were observed to be fiberlike or needlelike [shown later in Fig. 5(c)].

## RESULTS AND DISCUSSION

### Thermodynamic parameters

By the application of the Flory–Rehner equation,[25] the effect of the incorporation of an inorganic nanofiller on the crosslinking density of SBR can be estimated. Thermodynamic effects that occur during the swelling of the elastomer chains have also been analyzed. The elastic Gibbs free energy ($\Delta G$) for the SBR/nano-$CaSO_4$ composites has been determined with the Flory–Huggins equation[25] and with the statistical theory of rubber elasticity:

$$\Delta G = RT[\log(1 - \oslash_r) + \oslash_r + \chi(\oslash_r)^2]$$

where $\oslash_r$ is the volume fraction of the rubber composite and $\chi$ is 0.393 for toluene. $\Delta S$ can be obtained from $\Delta G = -T\Delta S$, which assumes that no change occurs in the internal energy of the networks upon stretching. Both thermodynamic parameters, $\Delta S$ and $\Delta G$, are reported in Table II. $\Delta G$ is −8.24 J/mol for pristine SBR, whereas −8.35, −9.73, and −17.09 J/mol have been recorded for 2 wt % 23-, 15-, and 10-nm $CaSO_4$/SBR composites, respectively. Commercial $CaSO_4$-filled SBR shows a $\Delta G$ value of −5.32 J/mol at the same weight percentage. Also, the values of $\Delta S$ are 0. 242, 0.268, and 0. 489 J/mol for 2 wt % 23-, 15-, and 10-nm $CaSO_4$/SBR composites, respectively, whereas $\Delta S$ is 0.163 J/mol for that weight percentage of the commercial $CaSO_4$ filler in SBR. The values of $\Delta G$ are −9.45, −15.79, and −19.93 J/mol for 12 wt % loadings of 23-, 15-, and 10-nm $CaSO_4$/SBR composites, whereas for commercial $CaSO_4$, the value of $\Delta G$ is −7.83 J/mol at the same loading. $\Delta G$ increases in the presence of commercial $CaSO_4$. However, a considerable decrease in the energy can be observed in nano-$CaSO_4$/SBR composites. It is assumed that $\Delta G$ is closely related to the elastic behavior of the material; nano-$CaSO_4$ shows better elasticity than commercial $CaSO_4$. These results show a better dispersion of nano-$CaSO_4$ throughout the matrix, giving rise to a process of intercalation. This intercalation is responsible for a noticeable increase in $\Delta S$ of the nano-$CaSO_4$/SBR composite. These results agree with results of Mousa and Karger.[26]

### Thermogravimetric analysis (TGA)

The thermal properties of pure SBR, commercial $CaSO_4$, and nano-$CaSO_4$ (23-, 15-, and 10-nm) SBR composites are summarized in Table II. The incorporation of nano-$CaSO_4$ into SBR with a reduced particle size shows better thermal stability than commercial $CaSO_4$-filled SBR. SBR filled with 23-, 15-, and 10-nm nano-$CaSO_4$ (2 wt %) shows decomposition temperatures of 445, 445, and 457°C, respectively, whereas the decomposition temperature is 440°C for the same weight percentage of commercial $CaSO_4$. The decomposition temperatures are 449, 456, and 469°C for 12 wt % loadings of 23-, 15-, and 10-nm $CaSO_4$, respectively, whereas for commercial $CaSO_4$, it is 442. The enhancement of the thermal stability is due to the uniform dispersion of nano-$CaSO_4$

**TABLE II**
**Thermodynamic Characteristics of Nano-$CaSO_4$-Filled and Commercial $CaSO_4$-Filled SBR Composites**

| Material | Filler (wt %) | $\Delta G$ (J/mol) | $\Delta S$ (J/mol) | TGA degradation peak (°C) | Weight loss (%)[a] |
|---|---|---|---|---|---|
| Pure SBR | 0 | −8.24 | $2.22 \times 10^{-1}$ | 439.89 | 92 |
| Nano-$CaSO_4$-filled SBR (23 nm) | 2 | −8.35 | $2.42 \times 10^{-1}$ | 445.30 | 90 |
| | 4 | −8.59 | $2.48 \times 10^{-1}$ | 445.84 | 89 |
| | 6 | −8.91 | $2.53 \times 10^{-1}$ | 446.37 | 88.58 |
| | 8 | −9.21 | $2.58 \times 10^{-1}$ | 447.74 | 88.42 |
| | 10 | −9.37 | $2.59 \times 10^{-1}$ | 448.96 | 86.85 |
| | 12 | −9.45 | $2.63 \times 10^{-1}$ | 449.00 | 85.00 |
| Nano-$CaSO_4$-filled SBR (15 nm) | 2 | −9.73 | $2.68 \times 10^{-1}$ | 445.45 | 87.00 |
| | 4 | −10.09 | $3.75 \times 10^{-1}$ | 446.90 | 83.00 |
| | 6 | −13.70 | $3.89 \times 10^{-1}$ | 450.67 | 84.00 |
| | 8 | −13.97 | $4.15 \times 10^{-1}$ | 452.00 | 81.00 |
| | 10 | −15.24 | $4.65 \times 10^{-1}$ | 455.23 | 80.52 |
| | 12 | −15.79 | $4.59 \times 10^{-1}$ | 456.21 | 80.00 |
| Nano-$CaSO_4$-filled SBR (10 nm) | 2 | −17.09 | $4.89 \times 10^{-1}$ | 457.23 | 84.00 |
| | 4 | −17.25 | $5.32 \times 10^{-1}$ | 460.23 | 82.00 |
| | 6 | −18.09 | $5.95 \times 10^{-1}$ | 462.56 | 81.25 |
| | 8 | −18.71 | $6.21 \times 10^{-1}$ | 463.23 | 80.00 |
| | 10 | −19.81 | $6.32 \times 10^{-1}$ | 465.12 | 79.00 |
| | 12 | −19.93 | $6.59 \times 10^{-1}$ | 469.23 | 78.85 |
| Commercial $CaSO_4$-filled SBR (20 μm) | 2 | −5.32 | $1.63 \times 10^{-1}$ | 439.92 | 92.00 |
| | 4 | −6.39 | $1.65 \times 10^{-1}$ | 440.23 | 90.00 |
| | 6 | −7.23 | $1.70 \times 10^{-1}$ | 441.01 | 89.58 |
| | 8 | −7.54 | $1.72 \times 10^{-1}$ | 441.12 | 89.40 |
| | 10 | −7.79 | $1.76 \times 10^{-1}$ | 442.02 | 89.00 |
| | 12 | −7.83 | $1.68 \times 10^{-1}$ | 442.23 | 88.00 |

[a] Amount of char residue.

throughout the matrix (as evident from SEM of the nanocomposites), which is responsible for the uniform absorption of heat and which prevents out-diffusion of the volatile decomposition product.[27]

## Swelling index

Figure 1 shows that the swelling index of nano-$CaSO_4$ is less than that of commercial $CaSO_4$-filled SBR. The swelling indices are 2.8, 2.03, and 1.88 for 2 wt % loadings of 23-, 15-, and 10-nm $CaSO_4$, respectively, whereas for commercial $CaSO_4$, it is recorded as 2.1. The swelling indices are 1.78, 1.68, and 1.45 for 23-, 15-, and 10-nm $CaSO_4$, respectively, at a 12 wt % loading; however, commercial $CaSO_4$-filled SBR shows a swelling index of 1.9. All these values are less than that of pristine SBR (2.12). The order of the swelling index with the particle size is 10 nm < 15 nm < 23 nm < commercial $CaSO_4$. This is due to the greater crosslinking of rubber as the uniform dispersion of nano-$CaSO_4$ brings the chains closer and keeps them intact with the nanoparticles. Swelling depends on the elastomer crosslinking density and solvent used. Figure 2 shows a schematic of the preferential migration of the solvent to the interface between the rubber chains and inorganic nanofiller, which is less in the nanofiller-filled SBR than in the commercial $CaSO_4$.

## Specific gravity

There is a continuous increment in the specific gravity for all compositions in comparison with pure SBR (Fig. 3). The increment in the specific gravity is more appreciable in the case of 10-nm $CaSO_4$ versus

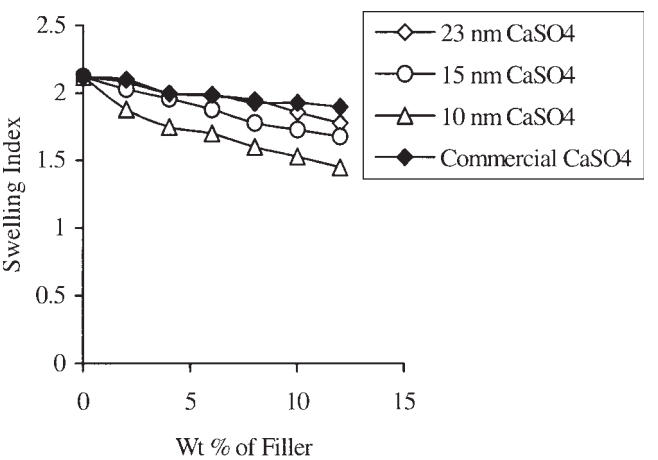


**Figure 1** Swelling index of SBR filled with various sizes and various weight percentages of $CaSO_4$ fillers.

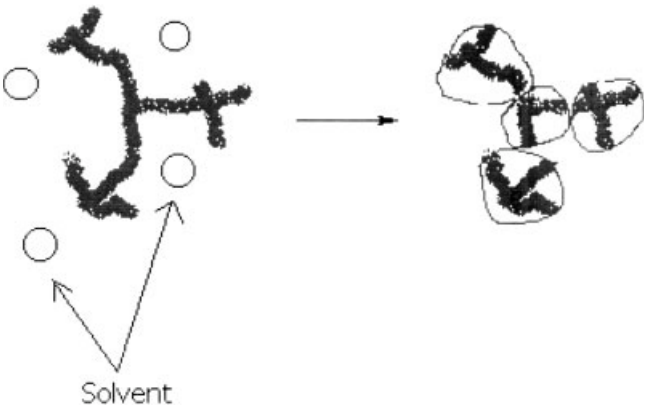


**Figure 2** Schematic of the preferential migration of the solvent to the interface of the rubber chains and inorganic nanofiller.

15-nm, 23-nm, and commercial $CaSO_4$ in SBR. The 2 wt % loading of 23-, 15-, and 10-nm $CaSO_4$ shows specific gravities of 0.93, 0.95, and 0.98, respectively, whereas for a 12 wt % loading of 23-, 15-, and 10-nm $CaSO_4$, the specific gravities are recorded as 1.16, 1.56, and 1.75, respectively. For 2 and 12 wt % loadings of commercial $CaSO_4$, the specific gravities are recorded as 0.92 and 0.99, respectively. The increase in the specific gravity with a reduction in the nanosize is due to the greater and uniform dispersion of the filler in the matrix, which keeps the rubber chains intact on crosslinking. Also, the free volume within the rubber chains is reduced because of the uniform dispersion of the nanoparticles and better crosslinking of rubber. These results complement the results of the swelling index.

### Tensile strength

The relation between the loading of the filler and the tensile strength of SBR filled with nano-$CaSO_4$ and commercial $CaSO_4$ is shown in Figure 4. The tensile strength increases with a reduction in the size of $CaSO_4$-filled SBR. A 2 wt % loading of 23-, 15-, and 10-nm $CaSO_4$ results in tensile strengths of 1.21, 1.24, and 1.4 MPa, respectively. The tensile strengths are recorded as 1.41, 1.78, and 2.31 MPa at a 10 wt % loading of 23-, 15-, and 10-nm $CaSO_4$, respectively, whereas 2 and 10 wt % loadings of commercial $CaSO_4$ show tensile strengths of 1.21 and 1.28 MPa. The results of the nanofillers are not appreciable above 10 wt % loadings because the nanoparticles become agglomerated at a higher weight percentage of $CaSO_4$. Inorganic nanoparticles are strongly fixed by electrostatic forces in rubber, so it is necessary to add a hydrophobic layer with a coupling agent to reduce the agglomeration problem.[22,23,28] This phenomenon can also be observed by SEM [Fig. 5(a,b)], which gives a clear idea of the agglomeration and uniform dispersion of the nanoparticles in the rubber matrix at 10 and 12 wt % loadings of the filler.

### Elongation at break

Figure 6 illustrates the elongation at break of nano-$CaSO_4$- and commercial $CaSO_4$-filled SBR. For all compositions, the elongation at break increases with an increase in the filler content up to 10 wt % and subsequently decreases with an increase in the filler content. The increment in the elongation at break in all nanosizes of $CaSO_4$ (23, 15, and 10 nm) is significantly greater than that of the commercial $CaSO_4$-filled SBR. However, the elongation at break is more appreciable in 10-nm $CaSO_4$ than in the other two sizes, 23 and 15 nm. The values of the elongation at break are 258, 275, and 320% at 2 wt % loadings of 23-, 15-, and 10-nm $CaSO_4$. However, a 10 wt % loading of the nanosizes shows 323, 372, and 415%

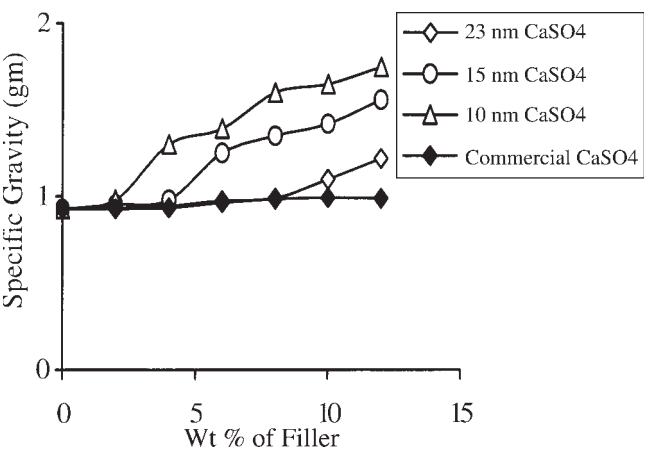


**Figure 3** Specific gravity of SBR filled with various sizes and various weight percentages of $CaSO_4$.

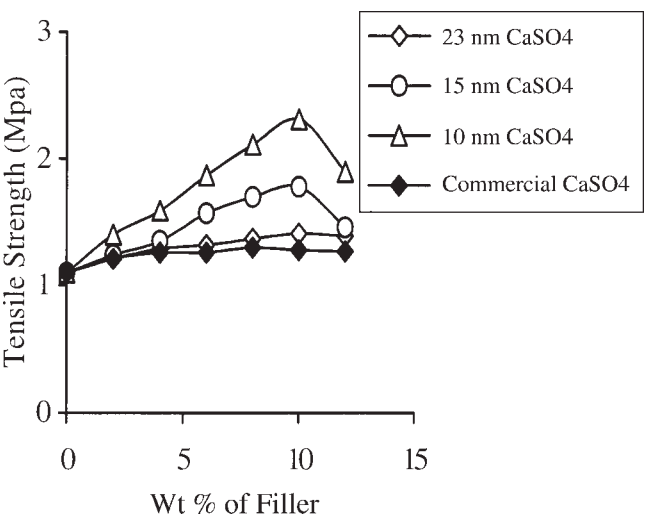


**Figure 4** Tensile strength of SBR filled with various sizes and various weight percentages of $CaSO_4$.

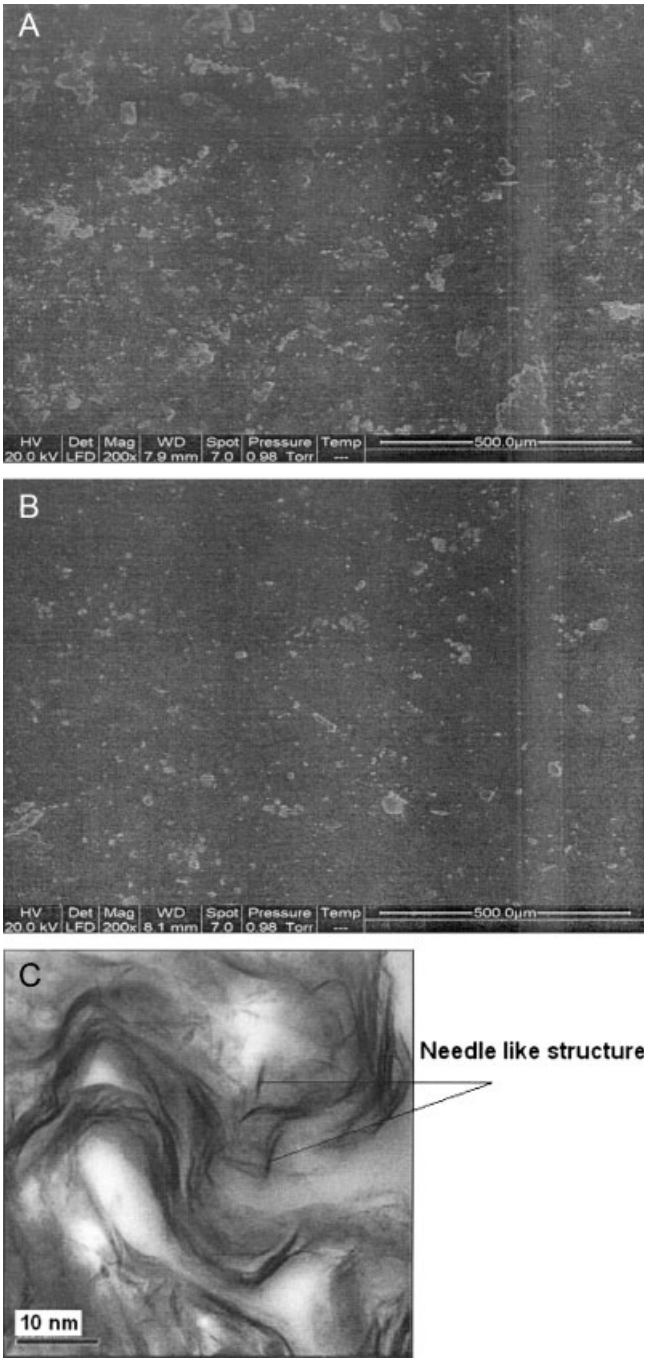


**Figure 5** (a) SEM of 10 wt % nano-$CaSO_4$-filled SBR, (b) SEM of 12 wt % nano-$CaSO_4$-filled SBR, and (c) TEM of $CaSO_4$ nanoparticles.

elongation at break. The elongations at break are 246 and 289% for 2 and 10 wt % loadings of commercial $CaSO_4$. Also, the elongation at break is recorded as 240% for pristine SBR, which is significantly less than those of the other compositions. This effect is due to the very fine size of the particles, which produce more interfacial bonding along with good dispersion and homogeneity in bonding. Manchando et al.[24] also observed this. Generally, the addition of a filler reduces the elongation of a composite;[27] however, the opposite trends are possible in some cases.

### Modulus at 300% elongation

The modulus at 300% elongation increases up to a 10 wt % filler loading for all compositions and subsequently decreases with an increasing amount of the filler (Fig. 7). This property is more appreciable for nano-$CaSO_4$ than commercial $CaSO_4$. Also, the modulus at 300% elongation is more pronounced in 10-nm $CaSO_4$ in comparison with 23- and 15-nm $CaSO_4$. Moduli at 300% elongation are recorded as 0.75, 0.85, and 1.25 MPa for 10 wt % loadings of 23-, 15-, and 10-nm $CaSO_4$, respectively, whereas 0.55 MPa is recorded for commercial $CaSO_4$. The decrement in the modulus at 300% elongation, above 10 wt % nano-$CaSO_4$-filled SBR, is due to the agglomeration of nanoparticles, which is evidenced by SEM [Fig. 5(a,b)], as mentioned earlier in the text. Kim et al.[28] also observed the same trend in nitrile rubber (NBR) nanocomposites based on organophilic layered clay.

### Young's modulus

The effect on Young's modulus by an increasing weight percentage and reduction in the nanosize of the $CaSO_4$ filler in SBR is shown in Figure 8. For all compositions, Young's modulus also increases up to a 10 wt % loading of the filler, and a further slight decrement is observed with the addition of the filler. The increment in Young's modulus with a reduction in the particle size of $CaSO_4$ (23, 15, and 10 nm) is significantly greater than that of the commercial $CaSO_4$ filler in SBR. However, a slight increment in Young's modulus can be observed for 10-nm $CaSO_4$ compared with 15- and 23-nm $CaSO_4$. Young's moduli are

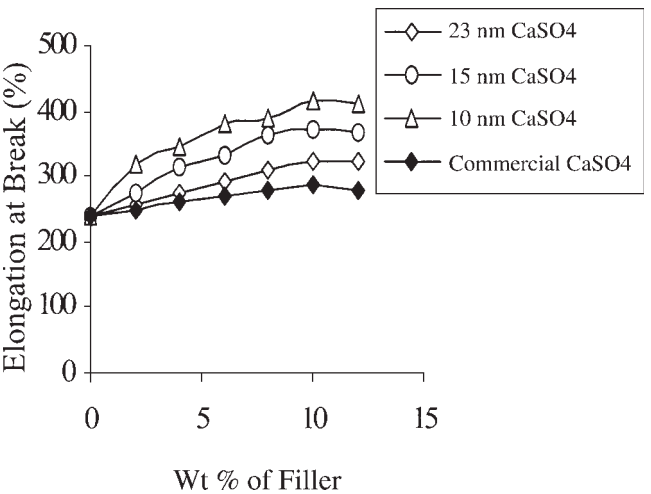


**Figure 6** Elongation at break of SBR filled with various sizes and various weight percentages of $CaSO_4$.

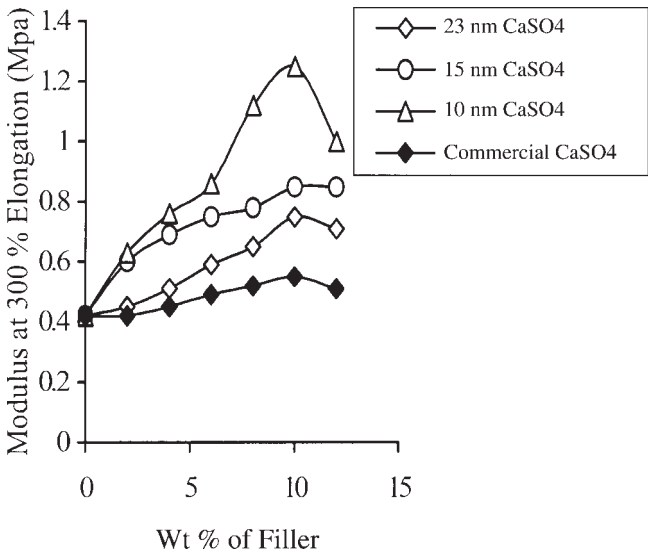


**Figure 7** Modulus at 300% elongation of SBR filled with various sizes and various weight percentages of $CaSO_4$.

recorded as 1.52, 1.64, and 1.72 MPa for 10 wt % additions of 23-, 15-, and 10-nm $CaSO_4$, respectively, whereas for that weight percentage of commercial $CaSO_4$, Young's modulus is recorded as 1.56 MPa.

Above a 10 wt % loading of nano-$CaSO_4$, Young's modulus decreases slightly or remains as it is.

## Flammability

Flammability can be inhibited or even suppressed by chemical or filler action. They interfere with the combustion during a particular stage of this process, that is, during heating or the spread of flames.[29,30] The rate of flame retardancy of different filler compositions is shown in Figure 9. The flame retardancy of nano-$CaSO_4$-filled SBR can be observed significantly in comparison with commercial $CaSO_4$. At 2 wt % loadings of 23-, 15-, and 10-nm $CaSO_4$, the

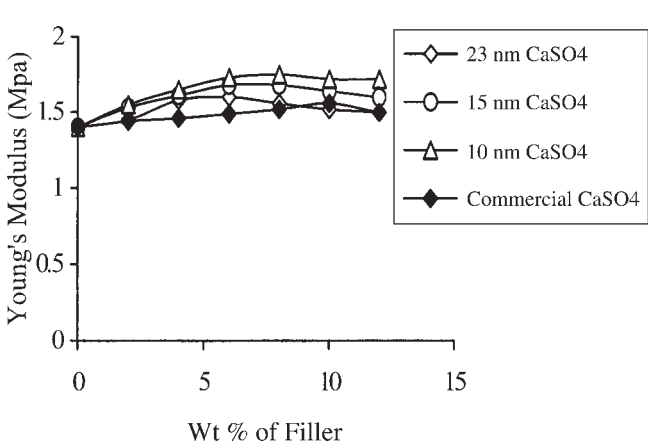


**Figure 8** Young's modulus of SBR filled with various sizes and various weight percentages of $CaSO_4$.

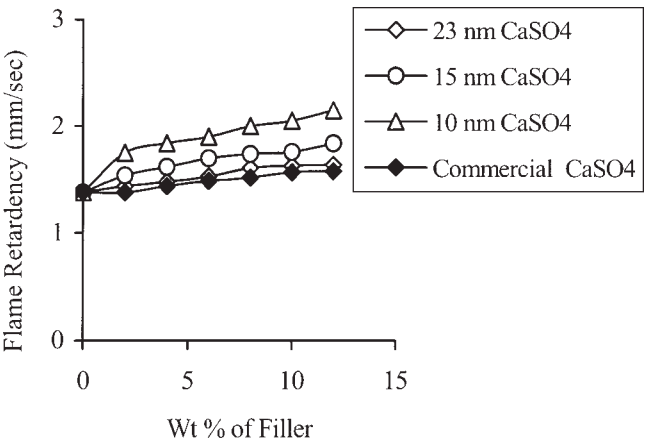


**Figure 9** Flame retardancy of SBR filled with various sizes and various weight percentages of $CaSO_4$.

flammability rates are found to be 1.44, 1.54, and 1.75 s/mm, respectively, whereas 12 wt % loadings of those sizes of $CaSO_4$ show 1.64, 1.84, and 2.15 s/mm, respectively; 2 and 12 wt % loadings of commercial $CaSO_4$ show rates of flammability of 1.58 and 1.38 s/mm, respectively. Thus, the absorption of energy by nanoparticles is uniform (endothermic). This effect drastically improves the burning resistance and absorbs the heat of burning. The nanoscale inorganic filler in the rubber nanocomposites promotes the formation of the char layer, which acts as an excellent insulator and mass-transfer barrier, because of which this effect drastically improves the burning resistance and absorbs the heat of burning. It has also been proved by the recorded amount of the char residue of the composites. The amount of the char residue increases with an increase in the amounts of the nanofillers; however, this increment is more in the case of smaller nanoparticles in comparison with bigger nanoparticles and commercial $CaSO_4$ (Table II). This insulating effect of the char

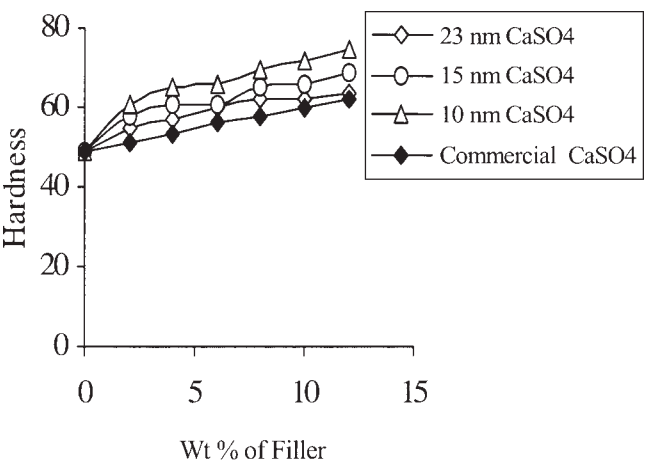


**Figure 10** Hardness of SBR filled with various sizes and various weight percentages of $CaSO_4$.

layer of the inorganic nanofiller slows down the escape of the volatile products generated by the decomposition of SBR. Also, the crucial parameter responsible for lowering the heat release rate of the rubber nanocomposites is the mass loss rate during combustion, which is significantly reduced for nanocomposites in comparison with pure SBR and commercially filled SBR composites. The lowering of the heat release rate is also due to the presence of inorganic nanoparticles between the chains of rubber, which first hinder the diffusion of volatile decomposition products from the nanocomposites and act as a barrier to the diffusion of oxygen into the nanocomposites at the same time. Also, SBR nanocomposites are thermally more stable than SBR filled with the commercial $CaSO_4$ filler.

### Hardness

Figure 10 shows the hardness of SBR filled with $CaSO_4$ versus variations in the weight percentage and reductions in the particle size. An increment can be observed in the hardness with an increase in the amount of the filler for all compositions, and it is more pronounced for nano-$CaSO_4$-filled SBR than commercial $CaSO_4$. Also the hardness increment is more in the case of 10-nm $CaSO_4$ than 23- and 15-nm $CaSO_4$. Upon the addition of 2 wt % loadings of 23-, 15-, and 10-nm $CaSO_4$, the hardness can be observed to be 55, 58 and 61, respectively. The values of the hardness are 64, 69, and 75 for 12 wt % loadings of 23-, 15-, and 10-nm $CaSO_4$, whereas the values of the hardness are recorded as 51 and 62 for 2 and 12 wt % loadings, respectively, of commercial $CaSO_4$ in SBR.

### Abrasion resistance

Nano-$CaSO_4$ shows greater abrasion resistance than commercial $CaSO_4$ (Fig. 11). The abrasion resistance indices are 0.3, 0.24, and 0.2 for 12 wt % loadings of 23-, 15-, and 10-nm $CaSO_4$, respectively, in SBR, respectively, whereas for that loading of commercial $CaSO_4$, the abrasion index is 0.39. This is due to the uniform dispersion of the nanofiller in the rubber matrix, which forms an effective layer that increases the crosslinking of the matrix. Thus, the degree of abrasion also decreases with a reduction in the nanosize of $CaSO_4$.

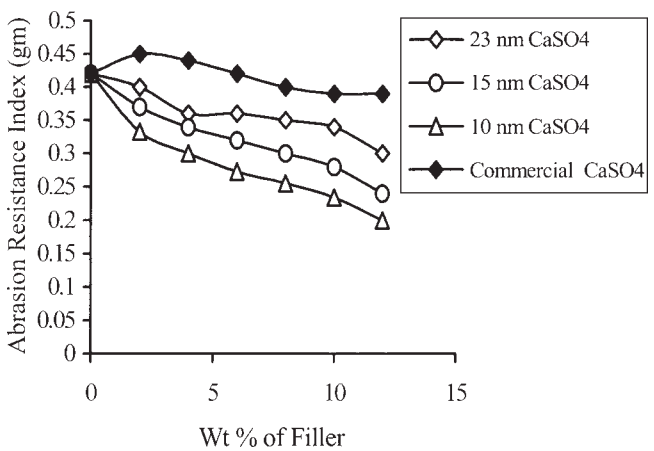


**Figure 11** Abrasion resistance index of SBR filled with various sizes and various weight percentages of $CaSO_4$.

It can be summarized from the results that the reduced nanosize of $CaSO_4$ provides better thermal, physical, and mechanical properties than commercial $CaSO_4$ in SBR. It can also be observed from a morphological study that the nanoparticles disperse uniformly throughout the matrix up to a 10 wt % filler loading and agglomerate at higher weight percentages in SBR. Swelling studies also support this result, as swelling decreases upon the reduction of the size of nano-$CaSO_4$. This might be due to greater crosslinking of rubber, as the uniform dispersion of nano-$CaSO_4$ brings the chains closer and keeps them intact with nanoparticles and thus more resistant to solvents than commercial $CaSO_4$, whereas reduced nanosizes show more enhancement in the specific gravity versus commercial $CaSO_4$. This is due to the uniform dispersion of the nanoparticles in the rubber chains, which reduces the free volume in the rubber matrix, which has already been discussed throughout the text. As the nanoparticles are so small that they disperse uniformly in the matrix and intercalate rubber chains to provide them with order, the surface area of the rubber chains increases. However, a higher amount of nano-$CaSO_4$ may get agglomerated; therefore, the behavior of the agglomerated part of nano-$CaSO_4$ may be assumed to be commercial $CaSO_4$, which is less dispersed in comparison with nano-$CaSO_4$ in the matrix.

## CONCLUSIONS

The following conclusions can be drawn from this study:

1. Physical properties such as the swelling index and specific gravity are much improved in nano-$CaSO_4$-filled SBR in comparison with commercial $CaSO_4$-filled SBR.
2. The tensile strength, elongation at break, and modulus at 300% elongation are greater up to 10 wt % nano-$CaSO_4$ in comparison with commercial $CaSO_4$ in SBR composites.
3. The rate of flammability is more reduced in nano-$CaSO_4$-filled rubber composites than in commercial $CaSO_4$-filled rubber composites.
4. The improvement in the properties is due to the uniform dispersion of nano-$CaSO_4$, which

brings the chains closer and keeps them intact with nanoparticles.

5. The mechanical properties of the rubber nanocomposites are not appreciable above 10 wt % filler because nano-$CaSO_4$ becomes agglomerated at higher percentages, which is evidenced by SEM of the rubber nanocomposites.

## References


1. Usuki, A.; Kojima, Y.; Okada, A.; Kamigaito, O. J Mater Res 1993, 8, 1185.
2. Lan, T.; Pinnavaia, T. J. J Chem Mater 1999, 6, 2216.
3. Brunside, S. D.; Giannelis, E. P. Chem Mater 1995, 7, 1597.
4. Vaia, R. A.; Vasudevan, S.; Krawice, W.; Scanlon, L. G.; Giannelis, E. P. Adv Mater 1995, 7, 154.
5. Gilman, J. W. Appl Clay Sci 1999, 15, 31.
6. Tong, X.; Zhaw, H.; Tang, T.; Feng, Z.; Huang, B. J Polym Sci Part A: Polym Chem 2002, 40, 1706.
7. Sinha, R. S.; Yamada, K.; Ogani, A.; Okamoto, M.; Idea, K. Macromol Rapid Commun 2002, 23, 943.
8. Sadhu, S.; Bhowmick, A. K. Rubber Chem Technol 2003, 76, 860.
9. Chang, Y. C.; Yang, Y.; Ryu, S.; Nah, C. Polym Int 2002, 51, 319.
10. Rong, J.; Jing, Z.; Li, H.; Sheng, M. Macromol Rapid Commun 2001, 22, 329.
11. Hung, X.; Brittain, W. J. Macromolecules 2001, 34, 3255.
12. Agag, T.; Koga, T.; Takeichi, T. Polymer 2000, 41, 7083.
13. Tyan, H. L.; Wei, K. H.; Hsieh, T. E. J Polym Sci Part B: Polym Phys 2000, 38, 2873.
14. Zheng, C.; Lee, L. J. Macromolecules 2001, 34, 4098.
15. Vergese, S.; Kager-Kocsis, J. Polymer 2003, 44, 4921.
16. Saujanya, C.; Radhakrishan, S. Polymer 2001, 42, 6723.
17. Heinemann, P.; Reichert, R.; Thomann, R.; Mulhaupt, R. Macromol Rapid Commun 1999, 20, 423.
18. Sadhu, S.; Bhowmick, A. K. Rubber Chem Technol 2003, 76, 860.
19. Mishra, S.; Sonawane, S. H.; Singh, R. P.; Bendale, A.; Patil, K. J Appl Polym Sci 2004, 94, 116.
20. Mishra, S.; Sonawane, S. H.; Singh, R. P. J Polym Sci Part B: Polym Phys 2005, 43, 107.
21. Mishra, S.; Sonawane, S. H.; Badgujar, N.; Gurav, K.; Patil, D. J Appl Polym Sci 2005, 96, 6.
22. Mishra, S.; Shimpi, N. G. J Sci Ind Res 2005, 41, 744.
23. Mishra, S.; Shimpi, N. G. J Appl Polym Sci 2005, 98, 2563.
24. Manchando, M. A.; Herrero, B.; Arroyo, M. Polym Int 2003, 52, 1070.
25. Flory, P. J. Principles of Polymer Chemistry; Cornell University: Ithaca, NY, 1953.
26. Mousa, A.; Karger, K. J. Macromol Mater Eng 2001, 286, 260.
27. Chem, G.; Lin, S.; Chen, S.; Qi, S. Macromol Chem Phys 2001, 202, 1189.
28. Kim, J.-T.; Oh, T.-S.; Lee, D.-H. Polym Int 2003, 52, 1058.
29. Usuki, A.; Okada, A. Mater Sci Eng C 1995, 3, 109.
30. Giannelis, E. NIST Grant Q Rep 1998, 8, 29.